Combustion and Flame 210 (2019) 236–246

Contents lists available at ScienceDirect

Combustion and Flame

journal homepage: www.elsevier.com/locate/combustflame

Experimental and kinetic modeling investigation on the laminar flame propagation of ammonia under oxygen enrichment and elevated pressure conditions

Bowen Mei[1], Xiaoyuan Zhang[1], Siyuan Ma, Mingli Cui, Hanwen Guo, Zhihao Cao, Yuyang Li*

Key Laboratory for Power Machinery and Engineering of MOE, Shanghai Jiao Tong University, Shanghai, 200240, PR China

ARTICLE INFO

Article history:
Received 19 May 2019
Revised 22 August 2019
Accepted 23 August 2019
Available online 6 September 2019

Keywords:
Ammonia
Laminar burning velocity
Oxygen enrichment
Elevated pressure
Kinetic model

ABSTRACT

Ammonia is attracting more and more attentions due to its role as both a carbon-free fuel for gas turbines and an effective H_2 carrier. Only a limit number of investigations on the laminar flame propagation and laminar burning velocity of ammonia have been performed on elevated pressures, which were focused on ammonia/air mixtures and suffered strong buoyancy effect. In this work, laminar flame propagation of ammonia/O_2/N_2 mixtures covering wide ranges of equivalence ratios, oxygen contents and initial pressures was investigated in a high-pressure constant-volume cylindrical combustion vessel. The oxygen enrichment speeds up the spherically expanding flames and consequently reduces buoyancy effect on the laminar flame propagation of ammonia. The laminar burning velocity was observed to increase with the increasing oxygen content, but decrease with the increasing initial pressure. A kinetic model of ammonia combustion consisting 38 species and 265 reactions was constructed from previous models with updated rate constants of important reactions. The present model can reasonably reproduce the laminar burning velocity data in this work and literature, as well as the ignition delay time and speciation data in literature. Based on the model analysis, effects of oxygen enrichment, equivalence ratio and initial pressure on laminar burning velocities of ammonia were analyzed in detail. It is revealed that the enhanced flame propagation with oxygen enrichment is mainly due to the increase of adiabatic flame temperature which in turn leads to higher concentrations of key radicals like H, OH and NH_2. For NH_3 and its major decomposition products like NH_2 and NH, reactions with oxygenated species such as OH, O, O_2 and NO are generally more important in the lean flames, while the role of reactions with H, NH and NH_2 becomes crucial in the rich flames. The calculated pressure dependent coefficient indicates that NH_3/O_2/N_2 flames exhibit clear pressure dependence, while this pressure dependence is weaker than those of the hydrocarbon and biofuel flames.

1. Introduction

Carbon-free fuels like H_2 and ammonia (NH_3), known with no greenhouse gas emissions, have attracted more and more attentions [1]. NH_3 is also an effective H_2 carrier [2] since 17.8% of H_2 by weight can be stored in NH_3 molecules [3]. NH_3 has been considered as a potential fuel candidate for a long time since it has a well-established production, transportation and storage infrastructure [1]. Ahlgren et al. [4] compared the fuel power density for different fuels, which is a unit that considers both the power in the fuel and the energy required to transport in pipelines. They found that the fuel power density of NH_3 is more than an order of magnitude higher than that of H_2 and four times higher than that of methane, suggesting NH_3 is a promising fuel in pipeline transportation. However, the low combustion intensity of NH_3, e.g. narrow flammability range and slow flame propagation, still challenges its practical applications, which still needs additional efforts on the fundamental researches of NH_3 combustion.

Laminar burning velocity (LBV) is one of the most important combustion parameters and plays an important role in the validation of combustion kinetic models and the determination of turbulent flame speed [5,6]. Previous studies have been performed to measure the LBVs of NH_3/air mixtures, while most of which were carried out at atmospheric pressure, as can be seen from Table S1 in the *Supplementary Materials*. Zakaznov et al. [7] measured the LBVs of NH_3/air mixtures under ambient condition using cylindrical-tube method. Their results showed that a mixture with 23% NH_3 (ϕ = 1.07) has the maximum LBV value of 7 cm/s, while

* Corresponding author.
E-mail address: yuygli@sjtu.edu.cn (Y. Li).
[1] These authors contributed equally to this work.

https://doi.org/10.1016/j.combustflame.2019.08.033
0010-2180/

for the mixture close to the lower flammability limit (17–17.5% NH_3), the LBV value is 3 cm/s. Pfahl et al. [8] measured the LBVs of NH_3/air mixtures in a constant-volume combustion vessel. To minimize the buoyancy effect, the horizontal component of the flame motion was measured to determine the LBVs. Jabbour et al. [9] measured the LBVs of NH_3/air mixtures at ambient pressure and temperature using a vertical tube. Takizawa et al. [10] measured the LBVs of NH_3/air mixtures at atmospheric pressure and room temperature in a constant-volume combustion vessel. The flame propagation was measured using both direct and schlieren photography. A red NH_3/air flame was observed in direct photography. Ronney et al. [11] measured the LBVs of NH_3/air mixtures using a constant-volume cylindrical combustion vessel at five initial pressures (P_u) under microgravity conditions, i.e., 0.066, 0.132, 0.329, 1 and 1.974 atm. Their results showed that initial pressure only has little influence on the LBV values of NH_3/air mixtures. Recently, Hayakawa et al. [12] measured the LBVs and Markstein lengths of NH_3/air mixtures at 1, 3 and 5 atm and equivalence ratio (ϕ) of 0.9–1.2 using a constant-volume cylindrical combustion chamber. They found that the trends of LBVs of NH_3 with varying initial pressure and equivalence ratio are as the same as those of hydrocarbon fuels, which is different from the observation of Ronney et al. [11]. Very recently, Han et al. [13] measured the LBVs of NH_3/air, NH_3/H_2/air, NH_3/CO/air and NH_3/CH_4/air mixtures using heat flux method. In summary, it is recognized that the LBVs of NH_3/air mixtures are extremely low due to the weak reactivity and low adiabatic flame temperatures. As a result, the laminar flame propagation of NH_3/air mixtures is strongly affected by buoyancy effect, while great influence of experimental uncertainties can hardly be avoidable, especially at elevated pressures.

There are continuous efforts on the development of kinetic models for NH_3 [14–22]. Among them, Tian et al. [16] developed a kinetic model in 2009 and validated the model against their own speciation data in low-pressure premixed flames of $NH_3/CH_4/O_2$/Ar mixtures. However, this model's performance on predicting the LBVs of NH_3/air and CH_4/NH_3/air flames was found less satisfactory [12,23]. In the same year, Konnov et al. [18] reported a kinetic model based on their previous model [24]. But this model overpredicts the LBVs of NH_3/air flames [12,25]. Later Mathieu and Petersen [26] developed a model for NH_3 oxidation and validated it against their measured ignition delay time data. Nakamura et al. [21] developed a model and validated it against the speciation data in their flow reactor weak flames, as well as the ignition delay time and LBV data in literature. Recently, Glarborg et al. [20] developed a kinetic model for nitrogen chemistry with NH_3 sub-mechanism and evaluated rate constants of some key reactions based on experimental and high-level theoretical calculation results in literature. However, this model was not validated against LBVs. Shrestha et al. [19] developed a comprehensive model of NH_3 and validated the model against LBVs, ignition delay times and speciation data. Very recently, Okafor et al. [22] developed a reduced model from a detailed model for CH_4/NH_3/air flames. Based on the above review of literature, new experimental and kinetic modeling efforts on the laminar flame propagation of NH_3 under reduced buoyancy effect and elevated pressure conditions will benefit the understanding of NH_3 combustion chemistry.

Oxygen-enriched combustion technology can increase the combustion intensity and improve combustion efficiency [27–29], making it another approach to enhance the combustion intensity of NH_3 besides the H_2 addition [13,30–34]. This technology has been applied in the ammonia/natural gas combustion in a 10 kW scale test furnace [1]. Besides, the oxygen enrichment can accelerate flame propagation [29] which can benefit the LBV measurements and kinetic model validation of NH_3 at elevated pressures. However, there are only few previous investigations on oxygen-enriched laminar flame propagation of NH_3. In 2015, Takeishi et al. [35] measured the LBVs of $NH_3/(28\%O_2/72\%N_2)$, $NH_3/(30\%O_2/70\%N_2)$ and $NH_3/(35\%O_2/65\%N_2)$ mixtures at atmospheric pressure. Very recently, Liu et al. [36] measured the LBVs of NH_3/O_2 mixtures at room temperature under low to moderate pressures ($P_u = 0.2$–1.6 atm, $\phi = 0.4$–2). No oxygen-enriched laminar flame propagation study of NH_3 has been performed at pressure greater than 1.6 atm yet. In this work, LBVs of $NH_3/O_2/N_2$ mixtures were measured at various equivalence ratios, oxygen contents and initial pressures. A high-pressure constant-volume cylindrical combustion vessel was used to facilitate the LBV measurements at 1–5 atm. Effects of oxygen enrichment, equivalence ratio and initial pressure on the measured LBV results were analyzed in detail. A kinetic model of ammonia combustion was constructed from previous models with updated rate constants of important reactions. Performance of the present model and several previous models of NH_3 on simulating the LBV results was compared. Modeling analysis were also performed to provide insight into the effects of oxygen enrichment, equivalence ratio and initial pressure on laminar flame propagation of NH_3.

2. Experimental method

The laminar flame propagation of $NH_3/O_2/N_2$ mixtures was investigated in a high-pressure constant-volume cylindrical combustion vessel. Detailed description of the apparatus has been described elsewhere [37]. In brief, the apparatus mainly consists of a constant-volume cylindrical combustion vessel, a premixing vessel, a gas inlet system, a spark ignition system and a schlieren system. The combustion vessel has an inner diameter of 150 mm with an optical access of 75 mm diameter. The method in previous shock tube experiments of NH_3 [26,38] was adopted to reduce the influence of NH_3 absorption on metal surface. Partial pressure method was used to prepare the mixtures in the premixing vessel, while after the combustible mixture was prepared, it was fed into the combustion vessel. After spark ignition, a high speed camera with the spatial resolution of 480 × 480 pixels (corresponding to 75 × 75 mm^2 region) and operated at 12,000 fps was used to record the laminar flame propagation. The data processing method has been introduced in our previous work [37]. To eliminate the ignition and confinement effects [39–41], the range of flame radius from 10 mm to 23 mm was selected. To minimize the buoyancy effect, the horizontal component was measured to determine the LBV values of NH_3/air mixtures according to the experience of Pfahl et al. [8], while in the oxygen-enriched experiments, the vertical component was measured since the buoyancy effect was dramatically reduced. The method of uncertainty evaluation is referred to our previous work [37] and is briefly introduced in the *Supplementary Materials*.

In this work, NH_3 (purity 99.999%), synthetic air ($21\%O_2/79\%N_2$), O_2 (purity 99.999%) and N_2 (purity 99.999%) were provided by Shanghai Weichuang Standard Gas Analytical Technology Co., Ltd. LBV measurements of NH_3/air mixtures were performed at atmospheric pressure, 298 K and $\phi = 0.6$–1.5. Based on previous work [10,13], the equivalence ratio of a $NH_3/O_2/N_2$ mixture is calculated with the following reaction,

$$NH_3 + \frac{3}{4x}(xO_2 + yN_2) \rightarrow \left(\frac{1}{2} + \frac{3y}{4x}\right)N_2 + \frac{3}{2}H_2O \quad (1)$$

where x and y are the mole fractions of oxygen and nitrogen in the oxidizer (O_2/N_2 mixtures), respectively. The oxygen content is defined as the mole fraction of oxygen in the oxidizer. LBV measurements of $NH_3/O_2/N_2$ mixtures with different oxygen contents (25%–45%) were mainly conducted at atmospheric pressure and equivalence ratios of 0.7, 1.0 and 1.5. For a specific oxygen content ($35\%O_2/65\%N_2$) which has close adiabatic flame temperature (2060–2460 K) to typical hydrocarbon/air mixtures, the measurements are performed at $P_u = 1$–5 atm and $\phi = 0.6$–1.5.

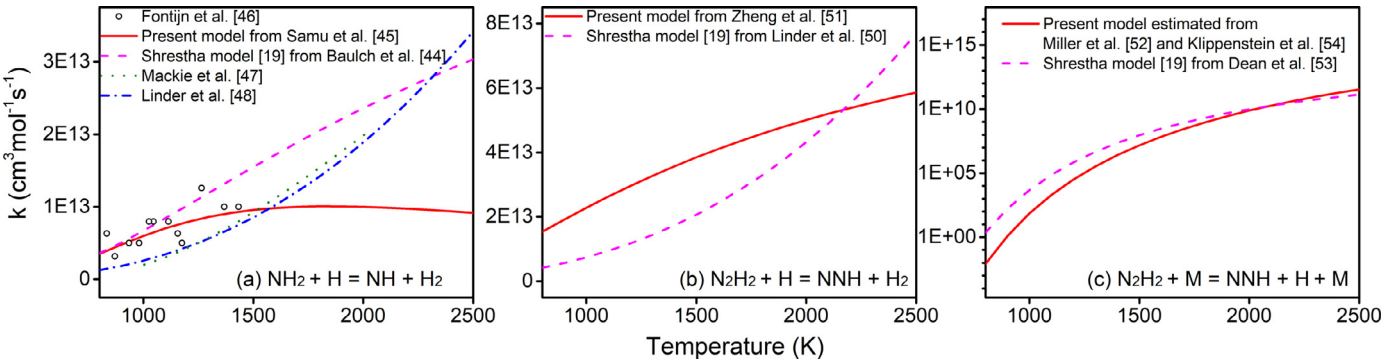

Fig. 1. Comparison of rate constants of (a) $NH_2 + H = NH + H_2$ (R5), (b) $N_2H_2 + H = NNH + H_2$ (R6) and (c) $N_2H_2 + M = NNH + H + M$ (R7) from different sources.

3. Kinetic modeling

In this work, a kinetic model was constructed from previous models with updated rate constants of important reactions. The base H_2 mechanism is adopted from a recent one of Hashemi et al. [42] and incorporated with the chemically termolecular reactions (R1-R4) [43]. The four reactions are very important for the LBV predictions of H_2 based on the studies of Burke and Klippenstein [43]. The NH_3 sub-mechanism is mainly taken from the model of Shrestha et al. [19] which shows better performance in the validation of literature data for NH_3 combustion. For the H abstraction reaction of NH_2 (R5), the rate constant at high temperatures still have large uncertainties [44–48]. In the model of Shrestha et al. [19], the rate constant of R5 was adopted from the earlier evaluation by Baulch et al. [44], which is 30%–43% higher than the measured result of Fontijn et al. [46] at above 1250 K. Previous theoretical calculation results from Linder et al. [48] and Mackie et al. [47] are close with each other but are generally half of the measured result of Fontijn et al. [46] at 870–1440 K. Very recently, Samu et al. [45] optimized the rate constant of R5 based on both the re-evaluated mole fraction of NH_2 which was originally measured in a NH_3 doped methane/air flame by their group [49] and the direct measurements and theoretical calculations of R5 in literature. According to Samu et al. [45], their rate constant is in good agreement with the measured result reported by Fontijn et al. [46] and can improve the prediction of NH_2 concentration profiles [49]. Therefore, in the present model, the rate constant reported by Samu [45] is adopted for R5. The comparison of rate constants of R5 from different sources is shown in Fig. 1(a). For R6, the model of Shrestha et al. [19] adopted earlier theoretical calculation rate constant reported by Linder et al. [50]. More recently, Zheng et al. [51] also calculated the rate constant of R6. They adopted multi-structural variational transition state theory with multidimensional tunneling and considered torsional anharmonicity using the multi-structural torsion method. Their obtained rate constant has a different temperature dependency compared with that calculated by Linder et al. [50]. Below 2200 K, the calculated result of Zheng et al. [51] is higher than that of Linder et al. [50], while above 2200 K, the calculated result of Linder et al. [50] is higher than that of Zheng et al. [51]. In the present model, the recent calculated result of Zheng et al. [51] is adopted for R6. The comparison of rate constants of R6 from different sources is shown in Fig. 1(b). For the unimolecular decomposition reaction of N_2H_2 (R7), investigations on the measured and calculated rate constants are limited. Miller and Bowman [52] evaluated the rate constant of R7 in their review paper of nitrogen chemistry. Dean et al. [53] roughly calculated the rate constant of R7 based on an estimated energy barrier. Klippenstein et al. [54] calculated the potential energy surface of the decomposition of N_2H_2 with high-level theoretical methods but did not report the rate constants. In this work, we estimated the rate constant of R7 from the evaluated result of Miller and Bowman [52] with the energy barrier adjusted according to the calculated result of Klippenstein et al. [54]. The comparison of rate constants of R7 from different sources is shown in Fig. 1(c).

$$H + O_2 + H = H_2 + O_2 \quad (R1)$$

$$H + O_2 + H = OH + OH \quad (R2)$$

$$H + O_2 + O = OH + O_2 \quad (R3)$$

$$H + O_2 + OH = H_2O + O_2 \quad (R4)$$

$$NH_2 + H = NH + H_2 \quad (R5)$$

$$N_2H_2 + H = NNH + H_2 \quad (R6)$$

$$N_2H_2 + M = NNH + H + M \quad (R7)$$

In this work, previous models developed by Tian et al. [16], Mathieu and Petersen [26], Nakamura et al. [21], Glarborg et al. [20], Shrestha et al. [19] and Okafor et al. [22] will be referred as the Tian model, the Mathieu model, the Nakamura model, the Glarborg model, the Shrestha model and the Okafor model in the following discussion, respectively. The present model and the six previous models were used to simulate the LBV data measured in this work. The simulation of LBVs in this work was performed with the Premixed Laminar Flame-Speed Calculation module of the Chemkin Pro-software [55]. All the simulations were converged to a grid-independent solution and the thermal diffusion effects were considered in this work. Furthermore, the ignition delay time data of $NH_3/O_2/Ar$ [26] and speciation data in a laminar premixed flame of $NH_3/H_2/O_2/Ar$ [58] and jet stirred reactor oxidation of $H_2/O_2/N_2/NO$ [59] in literature were also simulated with the present model and previous models. The simulation of ignition delay time in this work was performed with the Close Homogeneous Batch Reactor module of the Chemkin Pro-software [55]. The shock tube is treated as a zero-dimensional adiabatic reactor with constant volume. The simulated ignition delay time is defined as the time at which the line drawn along the steepest rate-of-change of OH^* de-excitation curve intersects with the zero-concentration line [26]. The simulation of laminar premixed flame and jet stirred reactor oxidation was performed with the Premixed Laminar Burner-Stabilized Flame module and the Perfectly Stirred Reactor module in the Chemkin-Pro-software [55], respectively. The reaction mechanism, thermodynamic data and transport data files of the present model can be found in the *Supplementary Materials*.

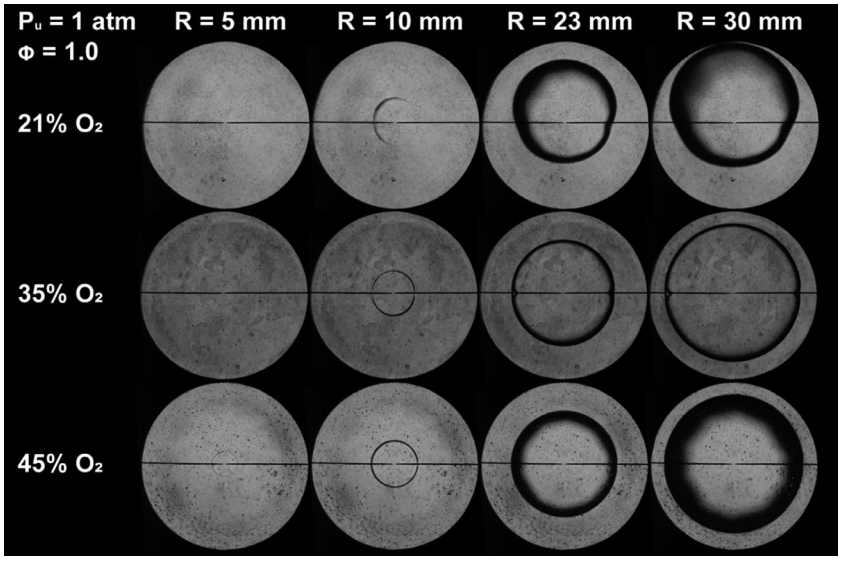

Fig. 2. Schlieren images of stoichiometric $NH_3/O_2/N_2$ flames with the oxygen content varying from 21% to 45% at $P_u = 1$ atm.

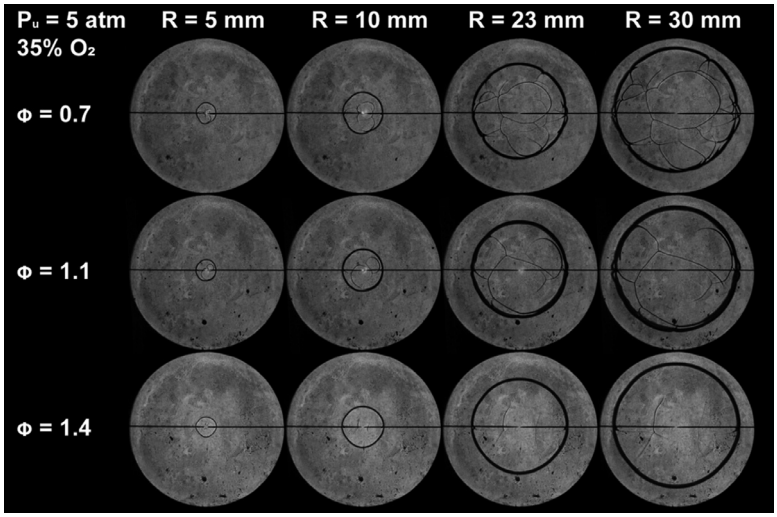

Fig. 3. Schlieren images of $NH_3/(35\%O_2/65\%N_2)$ flames at $P_u = 5$ atm and $\phi = 0.7$, 1.1 and 1.4.

4. Results and discussion

4.1. Measured and simulated results of LBVs

4.1.1. Flame morphology

Schlieren images of stoichiometric $NH_3/O_2/N_2$ flames at 1 atm under air and oxygen-enriched conditions are illustrated in Fig. 2. Similar to previous studies [8,10], the NH_3/air flame suffers severe buoyancy effect, as shown in the upper sub-figures of Fig. 2. The middle and lower sub-figures of Fig. 2 show that the buoyancy effect on the $NH_3/O_2/N_2$ flame is almost eliminated under oxygen-enriched conditions, as the flames with the oxygen contents (O_2 fraction in the O_2/N_2 mixture) of 35% and 45% are both nearly spherical.

Schlieren images of $NH_3/(35\%O_2/65\%N_2)$ flames at $\phi = 0.7$, 1.1 and 1.4 at 5 atm are illustrated in Fig. 3. Results show that the spherical flames under the rich conditions have smoother edges than those under the lean condition at the same flame radii, indicating that the onsets of cellular instability in lean $NH_3/(35\%O_2/65\%N_2)$ flames are lower than those in rich $NH_3/(35\%O_2/65\%N_2)$ flames. The measured Markstein lengths of $NH_3/(35\%O_2/65\%N_2)$ flames are shown in Fig. 4. At the same pressure, the Markstein length increases as ϕ increases. At the same equivalence ratio, it increases as the pressure increases at $\phi < 0.8$

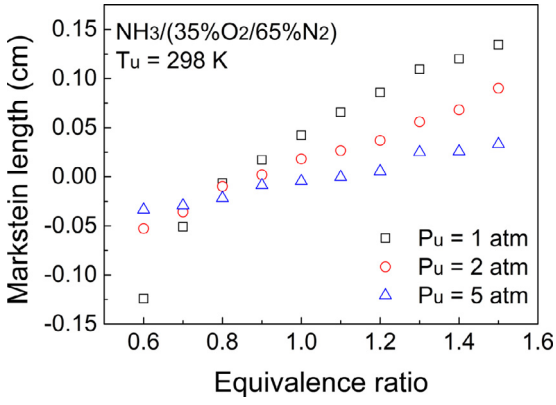

Fig. 4. Measured Markstein lengths of $NH_3/(35\%O_2/65\%N_2)$ flames at $T_u = 298$ K and $P_u = 1$, 2 and 5 atm.

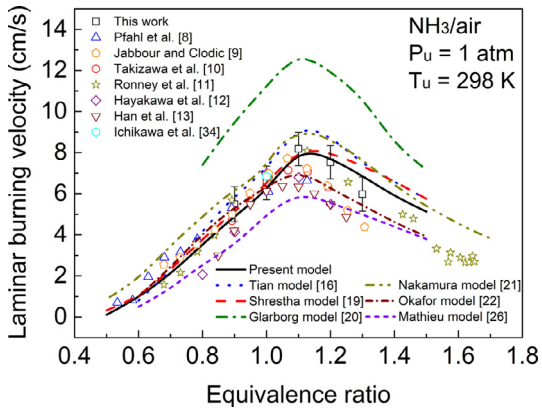

Fig. 5. LBVs of NH_3/air flames at $T_u = 298$ K and $P_u = 1$ atm. Symbols denote the measured results in this work and in literature [8–13,34], while lines denote the simulated results of the present model and previous models [16,19–22,26].

but decreases as the pressure increases at $\phi > 0.8$. This agrees with the experimental observations of H_2/air [56], CH_4/air [57] and NH_3/air [12] flames where the fuel is the lighter component in the combustible mixtures.

4.1.2. LBVs of NH_3/air mixtures

The measured LBVs of NH_3/air mixtures at $T_u = 298$ K and $P_u = 1$ atm in this work and literature work [8–12] are compared in Fig. 5. It can be observed that the measured LBVs of NH_3/air mixtures by different groups all peak around $\phi = 1.1$, while the maximum measured LBV values are between 6.6 and 8.1 cm/s. The measured results by different groups are in generally good agreement at ϕ less than 1.1, while discrepancies of about 2 cm/s appear at the rich side between these measured results. Therefore, it can be observed from Fig. 5 that the relative discrepancies at the rich side are quite apparent due to the low LBV values of NH_3/air mixtures.

The simulated results of the present model and six previous models are also plotted in Fig. 5. The simulated results using the Glarborg model start from $\phi = 0.8$ due to the difficult convergence at $\phi < 0.8$. Among the seven models, the Glarborg model and the Mathieu model have the highest and lowest predicted LBVs. The present model, the Tian model, the Nakamura model, the Shrestha model and the Okafor model can all predict the LBVs under the lean to stoichiometric conditions. More specifically, the simulated results of the Tian model and the Nakamura model are close to the upper boundary, while the present model, the Shrestha model and the Okafor model behave generally better. It is observed that the simulated results of the Glarborg model are always 3–5 cm/s higher than the measured results at $\phi < 1.1$, while the simulated results of the Mathieu model are always close to or exceed the lower boundary of measured results. Under the rich conditions, the Glarborg model still dramatically over-predicts the measured results, the Tian model, the Nakamura model and the Shrestha model all slightly over-predict the measured results, while the Okafor model, the Mathieu model and the present model can generally capture the measured results with consideration of experimental uncertainties.

It can be concluded that due to the extremely slow flame propagation, the LBV measurements of NH_3/air mixtures show great relative experimental uncertainties under the atmospheric pressure conditions. The seven NH_3 models have quite different performance on the predictions of LBVs of NH_3/air mixtures. Furthermore, the experimental uncertainties greatly affect the validation of NH_3 models. It could be imagined that for the LBVs of NH_3/air mixtures, the influence can become even greater under engine-relevant pressure conditions since the flame propagates much slower and relative experimental uncertainties become much greater at elevated pressures.

4.1.3. LBVs of $NH_3/O_2/N_2$ under various pressure and oxygen-enriched conditions

Figure 6 shows the measured and simulated LBVs of $NH_3/(35\%O_2/65\%N_2)$ mixtures at 298 K, pressures from 1 to 5 atm and ϕ from 0.6 to 1.5, while the comparison among the measured LBVs at the three pressures is shown in Fig. S1 of the *Supplementary Materials*. The results show that the LBV at the same pressure increases with ϕ under the lean conditions and decreases under the rich conditions, which is similar to the situation in the LBV measurements of NH_3/air mixtures [8–12]. At the three pressures, the peak values all appear at $\phi = 1.1$, which are also similar to the NH_3/air situation [8–12]. The peak values of the measured LBVs are 27.4, 24.8 and 21.4 cm/s at 1, 2 and 5 atm, respectively, which are much higher than the peak LBV values of NH_3/air mixtures. It can be concluded that the oxygen enrichment greatly accelerates the laminar flame propagation of NH_3. As shown in Fig. 6, the relative experimental uncertainties are well controlled under the oxygen-enriched conditions, even at elevated pressures, which can provide more stringent validation targets for NH_3 models.

Among the seven models, the Glarborg model and the Mathieu model over-predicts and under-predicts the LBVs of $NH_3/(35\%O_2/65\%N_2)$ mixtures within the whole measured pressure and ϕ ranges, respectively. The Tian model has better performance than the Glarborg model but still over-predicts the experimental results under whole conditions. The discrepancies between the measured results and simulated results of the Tian model increase with increasing pressure, which is reasonable since the Tian model was only validated against the species profiles in low-pressure (0.04 atm) premixed flames and lacks pressure-dependence for many pressure-dependent reactions [16]. The Okafor model over-predicts the LBVs of $NH_3/(35\%O_2/65\%N_2)$ mixtures under the lean conditions and under-predicts the peak equivalence ratio under all of the three pressures. The Nakamura model also slightly over-predicts the LBVs of $NH_3/(35\%O_2/65\%N_2)$ mixtures under the lean conditions at all of the three pressures. The Shrestha model behaves generally well under the lean conditions at the three pressures, while it under-predicts the measured results at 1 atm and $\phi = 1.0$–1.2 and slightly over-predicts the measured results at 5 atm and $\phi > 1.2$. Compared with previous models, the present model behaves generally better in simulating the LBVs of $NH_3/(35\%O_2/65\%N_2)$ mixtures within the whole measured pressure and ϕ range. Specifically, compared to the Shrestha model which is the base model for the NH_3 sub-mechanism of the present model, the present model improves the performance under the rich conditions at 1 and 2 atm. At 5 atm, similar to the Shrestha model, the present model also slightly over-predicts the LBVs at the rich side. Besides, the present model predicts almost the same as the Shrestha model under the lean conditions at the three pressures. Furthermore, the LBVs of $NH_3/(35\%O_2/65\%N_2)$ flame measured in this work and in the work of Takeishi et al. [35] at 1 atm and the simulated results by the present model and previous models are compared in Fig. S2 of the *Supplementary Materials*, which shows large discrepancies between the LBVs measured in the work of Takeishi et al. [35] and the rest measured and simulated results.

Figure 7 shows the measured LBVs of $NH_3/O_2/N_2$ mixtures as a function of oxygen content at 1 atm and $\phi = 0.7$, 1.0 and 1.5, as well as the simulated results of the present model and three previous NH_3 models which show generally better performance in simulating NH_3/air LBVs than other previous NH_3 models, i.e., the Shrestha model, the Nakamura model and the Okafor model. It can be observed that under the lean, stoichiometric and rich conditions, the oxygen enrichment can all greatly accelerate the laminar

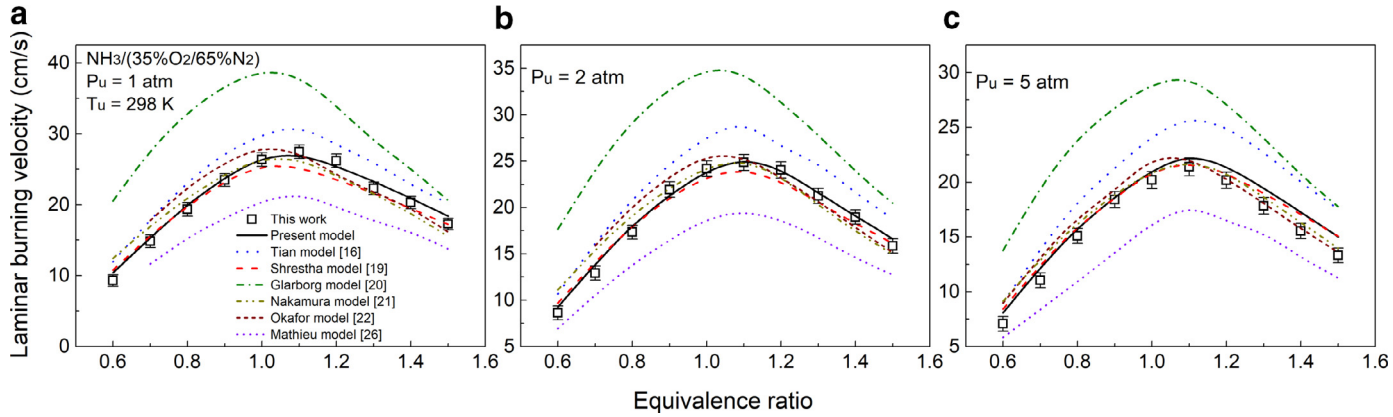

Fig. 6. LBVs of $NH_3/(35\%O_2/65\%N_2)$ mixtures at $T_u = 298$ K and $P_u = 1$–5 atm. The hollow square denotes the measured LBVs in this work, while lines denote the simulated results of the present model and previous models [16,19–22,26].

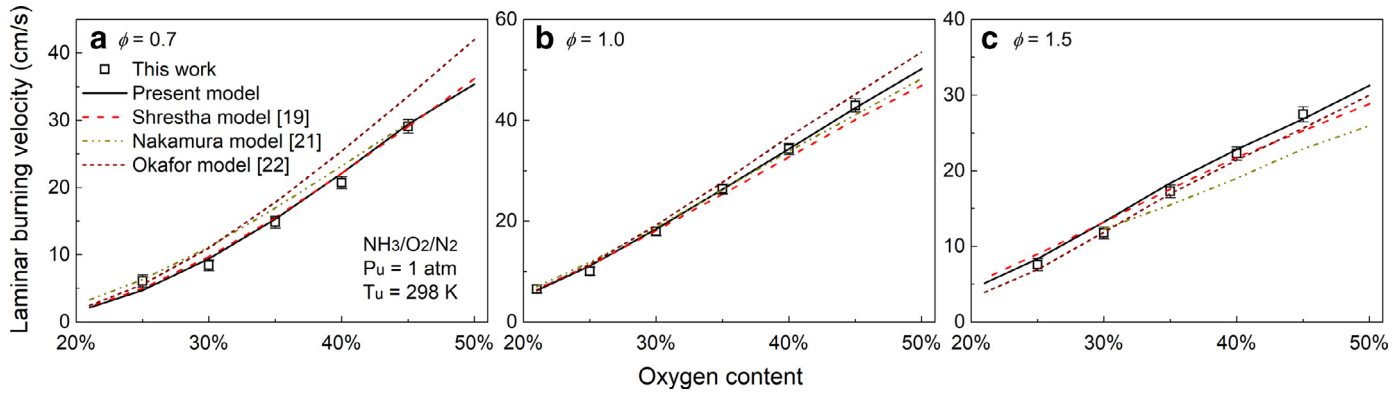

Fig. 7. LBV results of $NH_3/O_2/N_2$ mixtures at $T_u = 298$ K and $P_u = 1$ atm with different oxygen contents. The hollow square denotes the measured results in this work, while lines denote the simulated results of the present model, the Shrestha model [19], the Nakamura model [21] and the Okafor model [22].

flame propagation of NH_3. Among the three previous NH_3 models, the Shrestha model have a generally better performance under lean, stoichiometric and rich conditions. It can well capture the trend of LBVs versus oxygen content at $\phi = 0.7$. At $\phi = 1.0$, it behaves well when the oxygen content is less than 35%, but slightly under-predicts the LBVs when the oxygen content is greater than 35%. At $\phi = 1.5$, the simulated LBVs of the Shrestha model intersect with the measured results at 35% oxygen content. As shown in Fig. 7(a), the present model shows almost the same performance as the Shrestha model at $\phi = 0.7$. Compared to the Shrestha model, the present model can well capture the trends of LBVs versus oxygen content at $\phi = 1.0$ and 1.5, which can be seen from Fig. 7(b and c). To better demonstrate the improved performance of the present model under rich conditions, the present model and the Shrestha model are used to predict the ignition delay time data measured by Mathieu and Petersen [26] with $\phi = 2.0$ at various pressure as shown in Fig. 8. It can be observed from Fig. 8 that the present model has a generally better performance than the Shrestha model under the three rich conditions. Furthermore, validation of the present model on the speciation data of a laminar premixed $NH_3/H_2/O_2/Ar$ flame [58] and jet stirred reactor oxidation of $H_2/O_2/N_2/NO$ [59] in literature is shown in Figs. S3 and S4 of the *Supplementary Materials*.

4.2. Analysis of effects on LBVs

As can be observed from Figs. 6 and 7, the measured LBVs of $NH_3/O_2/N_2$ mixtures are affected by oxygen enrichment, equivalence ratio and initial pressure. To provide more insight into the effects of oxygen enrichment, equivalence ratio and initial pressure on the laminar flame propagation of $NH_3/O_2/N_2$ mixtures, modeling analyses including rate of production (ROP) analysis and sensitivity analysis are performed using the present model.

4.2.1. Effects of oxygen enrichment

As can be seen from the experimental and kinetic modeling results in Fig. 7, the oxygen enrichment generally leads to around an order of magnitude increase of LBV from the air conditions to the maximum oxygen content (45%) conditions. Figure 9 shows the ROP analysis results at 298 K and 1 atm under air and maximum oxygen content conditions. Under both conditions, NH_3 is almost totally consumed by H-atom abstraction reactions to form NH_2, especially by OH. NH_2 mainly react with H to form NH at $\phi = 0.7$, while the reaction with NH and self-combination to produce N_2H_2 become more important for the consumption of NH_2 at $\phi = 1.5$. NH_2 can also form NNH, H_2NO and HNO by reacting with NO, HO_2 and O, respectively. For NH, the reaction with NO to produce N_2O and the reaction with NH_2 to produce N_2H_2 are the main consumption pathways in the lean and rich flames, respectively, while it can also be converted to NO and N. For N_2H_2, it is mainly consumed by H-atom abstraction reactions and unimolecular decomposition reaction to form NNH, while NNH finally converts to N_2. Most H_2NO can also lose an H atom to produce HNO, while HNO almost totally decomposes to important pollutant NO. As can be observed from Fig. 9, the main pathways are identical under both NH_3/air and $NH_3/(45\%O_2/55\%N_2)$ conditions, while the contribution of each pathway varies as the oxygen content increases. For several main reaction pathways, the contributions demonstrate dramatic variations from air conditions to oxygen-enriched conditions. In particular, the contribution of H-atom

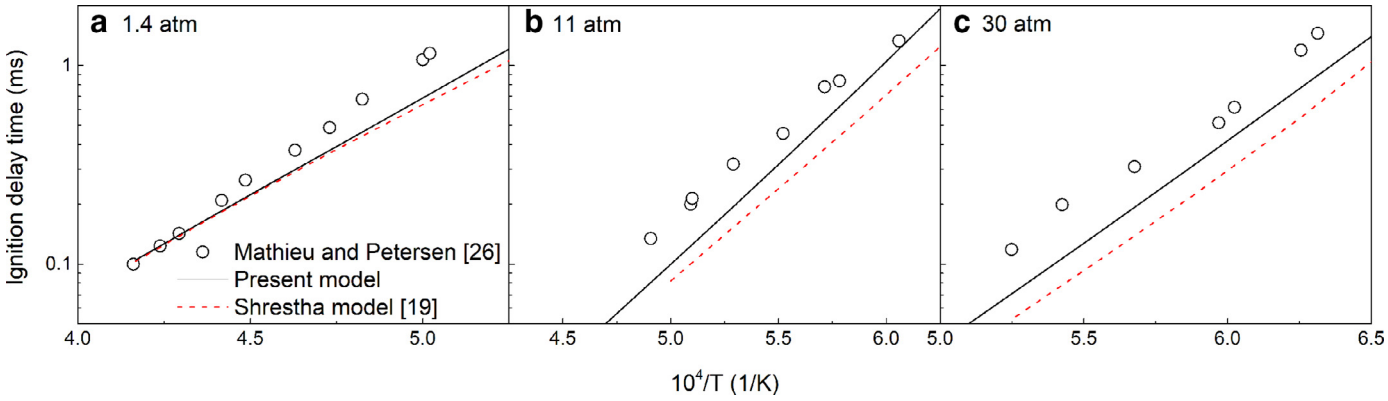

Fig. 8. Ignition delay time results of NH_3/O_2 mixtures diluted in 99% Ar with $\phi = 2.0$ at 1.4–30 atm. The hollow circle denotes the measured results in the work of Mathieu and Petersen [26], while lines denote the simulated results of the present model and the Shrestha model [19].

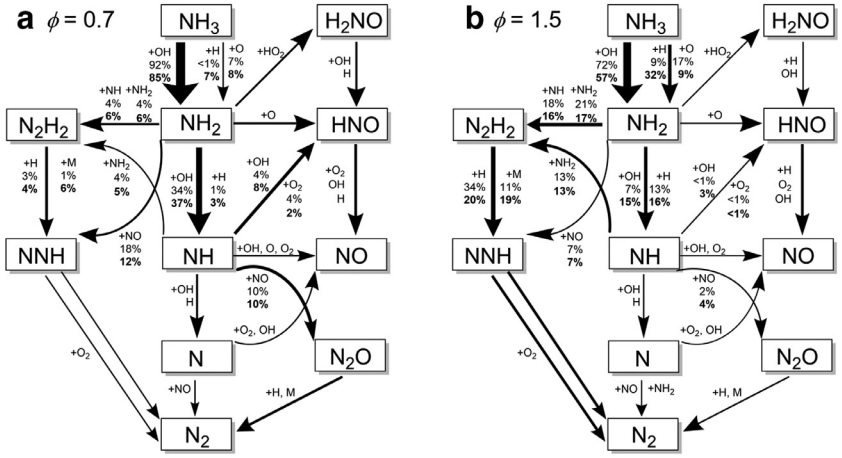

Fig. 9. Rate of production analysis in the lean (left, $\phi = 0.7$) and rich (right, $\phi = 1.5$) $NH_3/O_2/N_2$ flames under air (regular font) and maximum oxygen content ($45\%O_2/55\%N_2$, bold font) conditions at $T_u = 298$ K and $P_u = 1$ atm. For each pathway, the percentage and the thickness of arrow indicate the ratio of its reaction flux to the total reaction flux from the fuel.

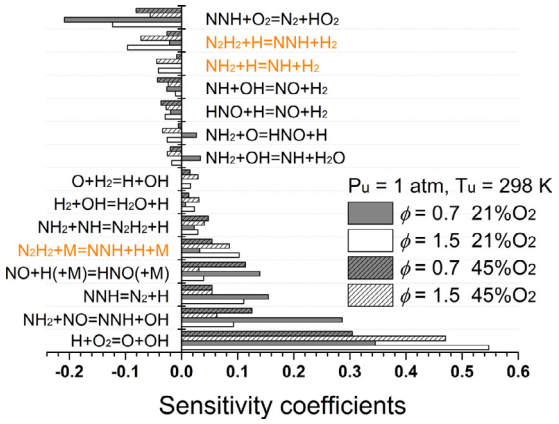

Fig. 10. Sensitivity analysis of LBV under the lean ($\phi = 0.7$, gray) and rich ($\phi = 1.5$, white) conditions with different oxygen contents ($21\%O_2$, empty; $45\%O_2$, slash) at $T_u = 298$ K and $P_u = 1$ atm. R5-R7 are marked in orange.

abstraction reaction of NH_3 by H under the maximum oxygen content conditions becomes more than 3 times than that under the air conditions, while the contribution of H-atom abstraction reaction of NH_3 by OH shows a reverse trend, as shown in Fig. 9.

Figure 10 shows the sensitivity analysis results at 298 K and 1 atm under air and maximum oxygen content conditions. Reactions in the H_2 sub-mechanism and the NH_3 sub-mechanism both exhibit high sensitivity coefficients for the laminar flame propagation of NH_3, especially $H + O_2 = O + OH$ which is also the most important high-temperature chain-branching reaction in hydrocarbon flames [6]. Similar to the ROP analysis, it can also be concluded from the sensitivity analysis that the sensitive reactions are the same in both air and oxygen-enriched flames, while the order of sensitivity coefficient varies slightly from the air conditions to the oxygen-enriched conditions.

To provide more insight into the effects of oxygen enrichment on the laminar flame propagation of $NH_3/O_2/N_2$ mixtures, the simulated adiabatic flame temperature and mole fractions of H, OH and NH_2 at $T_u = 298$ K, $P_u = 1$ atm and $\phi = 1.0$ using the present model are shown in Fig. 11. As expected, T_{ad} is greatly elevated as the oxygen content increases, that is, from 2051 K under the air condition to 2585 K under the maximum oxygen content condition. According to the study of Law et al. [60], the LBVs can be expressed as

$$S_u^0 \propto [(\gamma/c_p)Le]^{1/2}[exp(-E_a/R_0T_{ad})]^{1/2} \quad (2)$$

while T_{ad} here represents the thermal effect on the LBVs. Thus, the thermal effect of oxygen enrichment plays a predominant role in the increase of the LBVs of $NH_3/O_2/N_2$ mixtures, which is similar to the situations in the oxygen-enriched combustion of hydrocarbon fuels [29]. On the other hand, the mole fractions of the three key radicals in the $NH_3/O_2/N_2$ flames also rapidly increase with increasing oxygen content, which verifies that the elevated oxygen

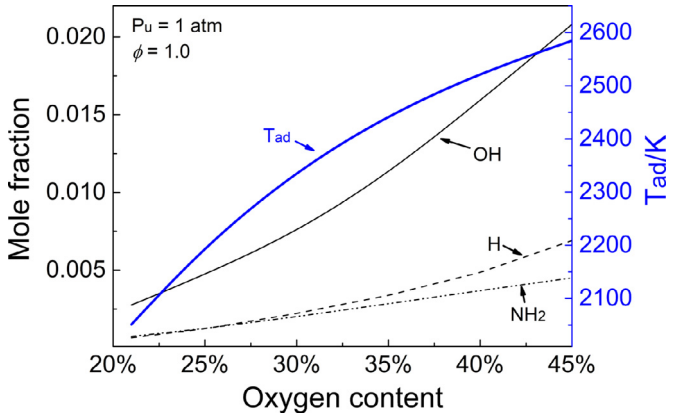

Fig. 11. Simulated adiabatic flame temperature and mole fractions of key radicals with different oxygen contents at $T_u = 298$ K, $P_u = 1$ atm and $\phi = 1.0$ using the present model.

content increases the mixture's reactivity and accelerates the laminar flame propagation.

4.2.2. Effects of equivalence ratio

As can be seen from Fig. 9, the importance of reaction pathways varies with equivalence ratios. Two equivalence ratios, $\phi = 0.7$ and 1.5, are used to represent the lean and rich conditions. Under the lean conditions, the consumption of NH_3 is dominated by the H-atom abstraction reaction by OH, while under the rich conditions, the contribution of the H-atom abstraction reaction by H increases dramatically. In particular, its contribution in the rich flame with 45% oxygen content becomes comparable to the H-atom abstraction reaction by OH. For NH_2, the contribution of its H-atom abstraction reaction by OH is more than an order of magnitude greater than that by H under the lean conditions, while the contributions of the two reactions become comparable under the rich conditions. Among the rest main consumption pathways of NH_2, the one producing N_2H_2 through both the self-combination and the reaction with NH has greatly increasing contributions from the lean flames to the rich flames. For NH, the reaction with NH_2 forming N_2H_2 becomes its most important consumption pathway in the rich flames, while the reactions with OH, NO and O_2 forming HNO, N_2O and NO are much more important in the lean flames. In conclusion, for NH_3 and its major decomposition products like NH_2 and NH, the reactions with oxygenated species such as OH, O, O_2 and NO are generally more important in the lean flames, while the role of the reactions with H, NH and NH_2 becomes crucial in the rich flames.

Three nitrogenous species reactions (R5-R7) with updated rate constants in the present model are marked in orange in Fig. 10. It is obvious that these reactions have much larger sensitivity coefficients under the rich conditions than under the lean conditions, which means that the laminar flame propagation of $NH_3/O_2/N_2$ mixtures is much more sensitive to R5-R7 under the rich conditions while less sensitive to them under the lean conditions. Figure 12 shows the predictions of the present model, the present model without updating R5-R7 and the Shrestha model on the LBV measurements of $NH_3/O_2/N_2$ mixtures at $T_u = 298$ K and $P_u = 1$ atm with different oxygen contents. It is clear that the three models predict closely under the lean condition. However, under the stoichiometric and rich conditions, the trends of the simulated results of the present model without updating R5-R7 is more similar to those of the Shrestha model, indicating that the update of the rate constants of R5-R7 helps improve the present model's performance. Furthermore, the slightly better performance of the present model without updating R5-R7 than that of the Shrestha model reveals the contribution of updating H_2 mechanism [42,43] to improve the present model's prediction ability.

4.2.3. Effects of initial pressure

As introduced in the Introduction section, there are some different opinions on the effects of initial pressure in the LBV measurements of NH_3/air mixtures. Ronney et al. [11] found that initial pressure only has little effect on the LBV values of NH_3/air mixtures under microgravity conditions at initial pressures from 0.066 atm to 1.974 atm. However, Hayakawa et al. [12] found that the LBVs of NH_3/air mixtures decrease as the initial pressure increase from 1 atm to 5 atm, which is the same as the situations of hydrocarbon fuels. As can be seen from Fig. 6, the measured LBVs of $NH_3/(35\%O_2/65\%N_2)$ flames also show an apparent dependence of initial pressure, which is similar to the finding of Hayakawa et al. in the NH_3/air flames [12]. Figure 13 shows the measured LBVs of $NH_3/(35\%O_2/65\%N_2)$ mixtures at $T_u = 298$ K and $\phi = 0.7$, 1.0 and 1.5. The LBVs all decrease gradually with increasing pressure, showing similar pressure effects at different equivalence ratios. The decrease of the LBVs becomes weaker as the pressure increases. This observation is in accordance with that of Hayakawa et al. [12], but different from that of Ronney et al. [11].

The pressure dependent coefficient β of the measured LBVs of $NH_3/(35\%O_2/65\%N_2)$ mixtures is calculated according to the pressure dependence relation: $LBV(P_u) = LBV(P_0) \cdot (P_u/P_0)^{\beta}$ [61,62], where P_0 as the reference pressure equals to 1 atm in this work and β equals to $\frac{n}{2} - 1$, while n is the overall reaction

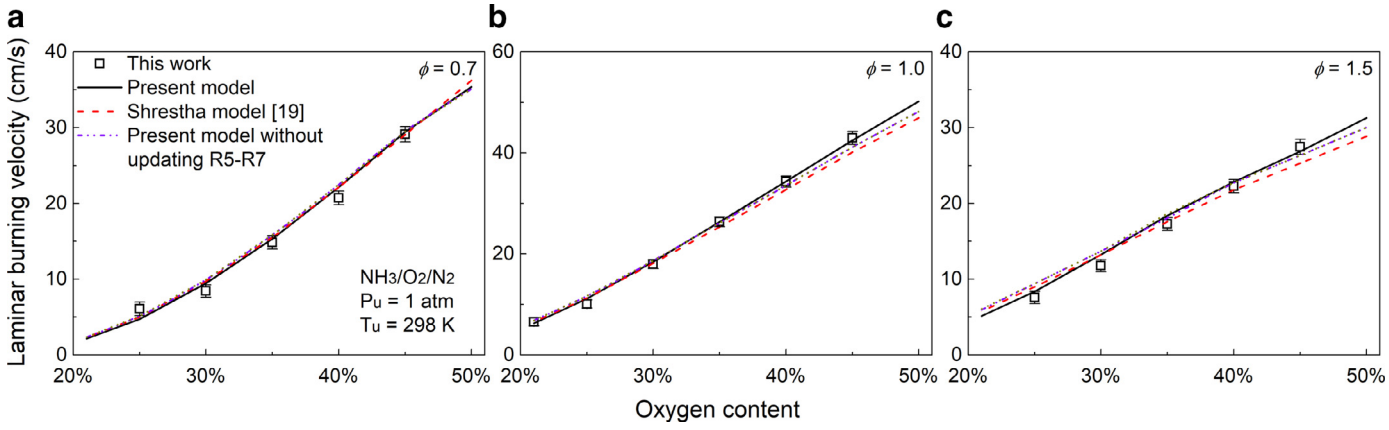

Fig. 12. Comparison of the simulated LBV results of the present model, the present model without updating R5-R7 and the Shrestha model [19] for $NH_3/O_2/N_2$ mixtures at $T_u = 298$ K and $P_u = 1$ atm with different oxygen contents.

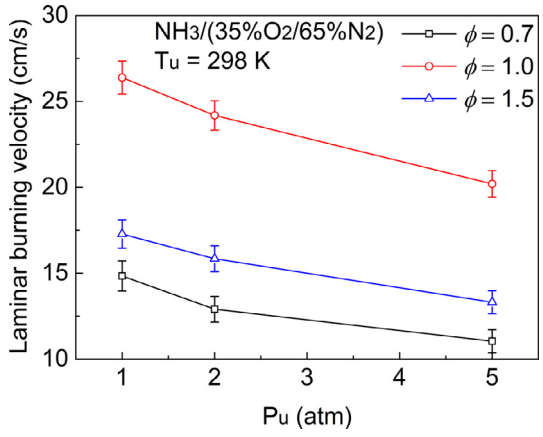

Fig. 13. Measured LBVs of $NH_3/(35\%O_2/65\%N_2)$ mixtures at $T_u = 298$ K and $\phi = 0.7$, 1.0 and 1.5.

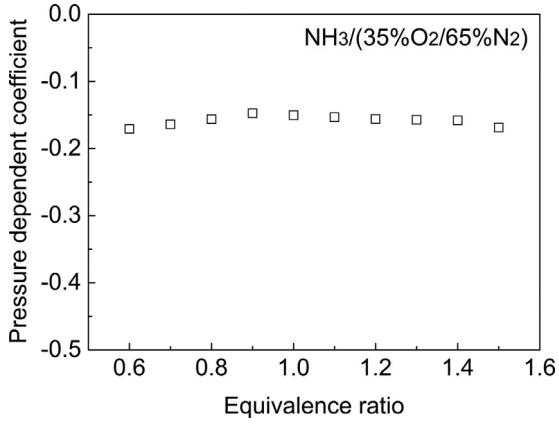

Fig. 14. Calculated pressure dependent coefficient β for $NH_3/(35\%O_2/65\%N_2)$ mixtures at $T_u = 298$ K.

order. Figure 14 shows the calculated pressure dependent coefficient β. As it shows, β of $NH_3/(35\%O_2/65\%N_2)$ mixtures of all calculated equivalence ratio range lie around −0.15, smaller than 0. It is in accordance with the conclusion drawn by Egolfopoulos et al. [61] that a burning flame dominated by two-body branching and carrying reactions should have an n close to 2 and the three-body termination reactions generally tend to reduce n. Furthermore, the β calculated in this work are larger than that of the methane/air flame [61,62], n-butanol/air and n-butanol/(14%O_2/86%He) flames [63], benzene/air, toluene/air and ethylbenzene/air flames [37] which means that the pressure effect is more obvious on hydrocarbon flames than on ammonia flames where there are more three-body termination reactions in hydrocarbon flames than ammonia flames. Furthermore, the sensitivity analysis for LBVs of $NH_3(35\%O_2/65\%N_2)$ mixtures at $T_u = 298$ K, $P_u = 1$, 2 and 5 atm and $\phi = 0.7$ and 1.5 using the present model is shown in Fig. 15. It can be observed that the sensitivity coefficients of most reactions vary little as initial pressure increases from 1 atm to 5 atm, implying that reactions in NH_3 combustion are not so sensitive to initial pressure as those in hydrocarbon and biofuel combustion [37,61,63]. This can be explained by the weak unimolecular decomposition of the fuel and combination reactions of radicals in NH_3 combustion, which are typical chain initiation and termination reaction classes and are responsible for the pressure dependence of LBV.

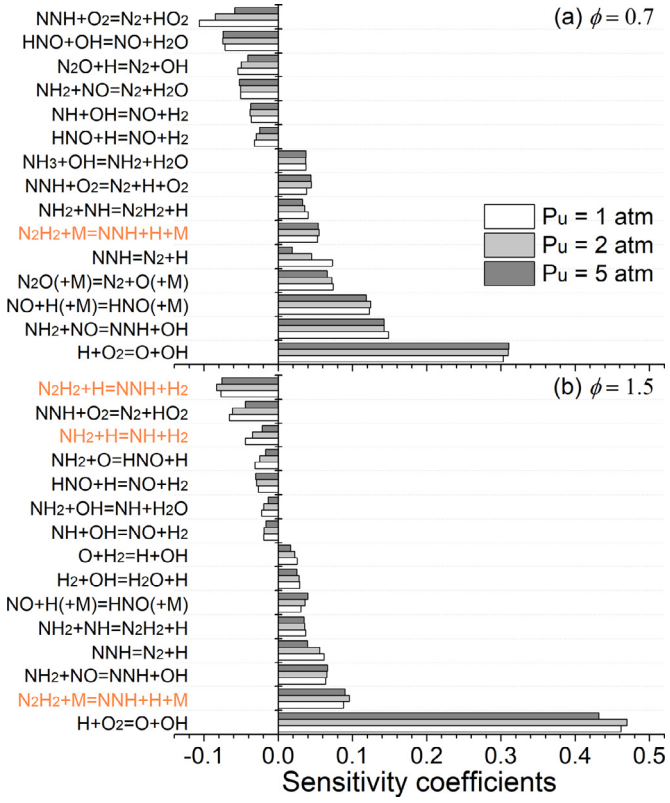

Fig. 15. Sensitivity analysis for LBVs of $NH_3(35\%O_2/65\%N_2)$ mixtures at $T_u = 298$ K, $P_u = 1$, 2 and 5 atm and $\phi =$ (a) 0.7 and (b) 1.5 using the present model. R5-R7 are marked in orange (For interpretation of the references to color in this figure legend, the reader is referred to the web version of this article.).

5. Conclusions

This work reports an experimental and modeling investigation on laminar flame propagation of $NH_3/O_2/N_2$ mixtures in a high-pressure constant-volume cylindrical combustion vessel. The flame morphology of NH_3/air and oxygen-enriched flames were compared, showing that the oxygen enrichment can accelerate the flame propagation and effectively minimize the buoyancy effect. As a result, the laminar burning velocities were observed to increase with the increasing oxygen content. A kinetic model of NH_3 combustion with 38 species and 265 reactions was constructed from previous models with updated rate constants of important reactions and validated against the LBV data in this work and literature, as well as the ignition delay time and speciation data in literature.

Modeling analysis such as ROP analysis and sensitivity analysis were performed to provide insight into the effects of oxygen enrichment, equivalence ratio and initial pressure. It is found that oxygen enrichment does not change the main reaction pathways in $NH_3/O_2/N_2$ flames, while the thermal effect plays a predominant role in the increase of the LBVs of $NH_3/O_2/N_2$ mixtures under oxygen-enriched conditions. Reactions in the H_2 sub-mechanism and the NH_3 sub-mechanism both exhibit high sensitivity coefficients for the laminar flame propagation of NH_3. Thus the development and update of both sub-mechanisms in this work ensure the good performance of the present model in predicting LBV and ignition delay time data of NH_3, especially under rich conditions. For NH_3 and its major decomposition products like NH_2 and NH, the reactions with oxygenated species such as OH, O, O_2 and NO are generally more important in the lean flames, while the role of the reactions with H, NH and NH_2 becomes crucial in the rich flames. Furthermore, the decrease of LBV with the

increasing initial pressure reveals the pressure dependence of the laminar flame propagation of $NH_3/O_2/N_2$ mixtures. The small absolute values of pressure dependent coefficient indicate that the pressure dependence of $NH_3/O_2/N_2$ flames is weaker than those of hydrocarbon and biofuel flames.

Acknowledgments

The authors are grateful for the funding support from National Key R&D Program of China (2017YFE0123100) and National Natural Science Foundation of1 China (51622605, 91841301, U1832171).

Supplementary materials

Supplementary material associated with this article can be found, in the online version, at doi:10.1016/j.combustflame.2019.08.033.

References

[1] H. Kobayashi, A. Hayakawa, K.D.K.A. Somarathne, E.C. Okafor, Science and technology of ammonia combustion, Proc. Combust. Inst. 37 (2019) 109–133.
[2] C. Zamfirescu, I. Dincer, Using ammonia as a sustainable fuel, J. Power Sources 185 (2008) 459–465.
[3] S. Chiuta, R.C. Everson, H.W.J.P. Neomagus, P. van der Gryp, D.G. Bessarabov, Reactor technology options for distributed hydrogen generation via ammonia decomposition: a review, Int. J. Hydrogen Energy 38 (2013) 14968–14991.
[4] W. Ahlgren, Fuel power density, J. Press. Vessel Technol. 134 (2012) 054504.
[5] J.F. Driscoll, Turbulent premixed combustion: flamelet structure and its effect on turbulent burning velocities, Prog. Energy Combust. Sci. 34 (2008) 91–134.
[6] E. Ranzi, A. Frassoldati, R. Grana, A. Cuoci, T. Faravelli, A.P. Kelley, C.K. Law, Hierarchical and comparative kinetic modeling of laminar flame speeds of hydrocarbon and oxygenated fuels, Prog. Energy Combust. Sci. 38 (2012) 468–501.
[7] V.F. Zakaznov, L.A. Kursheva, Z.I. Fedina, Determination of normal flame velocity and critical diameter of flame extinction in ammonia-air mixture, Combust. Explos. 14 (1978) 710–713.
[8] U.J. Pfahl, M.C. Ross, J.E. Shepherd, K.O. Pasamehmetoglu, C. Unal, Flammability limits, ignition energy, and flame speeds in H_2-CH_4-NH_3-N_2O-O_2-N_2 mixtures, Combust. Flame 123 (2000) 140–158.
[9] T. Jabbour, D.F. Clodic, Burning velocity and refrigerant flammability classification, ashrae transactions, Atlanta 110 (2004) 522–533.
[10] K. Takizawa, A. Takahashi, K. Tokuhashi, S. Kondo, A. Sekiya, Burning velocity measurements of nitrogen-containing compounds, J. Hazard. Mater. 155 (2008) 144–152.
[11] P.D. Ronney, Effect of chemistry and rransport properties on near-limit flames at microgravity, Combust. Sci. Technol. 59 (1988) 123–141.
[12] A. Hayakawa, T. Goto, R. Mimoto, Y. Arakawa, T. Kudo, H. Kobayashi, Laminar burning velocity and Markstein length of ammonia/air premixed flames at various pressures, Fuel 159 (2015) 98–106.
[13] X. Han, Z. Wang, M. Costa, Z. Sun, Y. He, K. Cen, Experimental and kinetic modeling study of laminar burning velocities of NH_3/air, NH_3/H_2/air, NH_3/CO/air and NH_3/CH_4/air premixed flames, Combust. Flame 206 (2019) 214–226.
[14] J.A. Miller, M.D. Smooke, R.M. Green, R.J. Kee, Kinetic modeling of the oxidation of ammonia in flames, Combust. Sci. Technol. 34 (1983) 149–176.
[15] R.P. Lindstedt, F.C. Lockwood, M.A. Selim, Detailed kinetic modelling of chemistry and temperature effects on ammonia oxidation, Combust. Sci. Technol. 99 (1994) 253–276.
[16] Z.Y. Tian, Y.Y. Li, L.D. Zhang, P. Glarborg, F. Qi, An experimental and kinetic modeling study of premixed $NH_3/CH_4/O_2$/Ar flames at low pressure, Combust. Flame 156 (2009) 1413–1426.
[17] Ø. Skreiberg, P. Kilpinen, P. Glarborg, Ammonia chemistry below 1400 K under fuel-rich conditions in a flow reactor, Combust. Flame 136 (2004) 501–518.
[18] A.A. Konnov, Implementation of the ncn pathway of prompt-NO formation in the detailed reaction mechanism, Combust. Flame 156 (2009) 2093–2105.
[19] K.P. Shrestha, L. Seidel, T. Zeuch, F. Mauss, Detailed kinetic mechanism for the oxidation of ammonia including the formation and reduction of nitrogen oxides, Energy Fuels 32 (2018) 10202–10217.
[20] P. Glarborg, J.A. Miller, B. Ruscic, S.J. Klippenstein, Modeling nitrogen chemistry in combustion, Prog Energ Combust Sci 67 (2018) 31–68.
[21] H. Nakamura, S. Hasegawa, T. Tezuka, Kinetic modeling of ammonia/air weak flames in a micro flow reactor with a controlled temperature profile, Combust. Flame 185 (2017) 16–27.
[22] E.C. Okafor, Y. Naito, S. Colson, A. Ichikawa, T. Kudo, A. Hayakawa, H. Kobayashi, Measurement and modelling of the laminar burning velocity of methane-ammonia-air flames at high pressures using a reduced reaction mechanism, Combust. Flame 204 (2019) 162–175.
[23] E.C. Okafor, Y. Naito, S. Colson, A. Ichikawa, T. Kudo, A. Hayakawa, H. Kobayashi, Experimental and numerical study of the laminar burning velocity of CH_4-NH_3-air premixed flames, Combust. Flame 187 (2018) 185–198.
[24] F.H.V. Coppens, J. De Ruyck, A.A. Konnov, The effects of composition on burning velocity and nitric oxide formation in laminar premixed flames of $CH_4 + H_2 + O_2 + N_2$, Combust. Flame 149 (2007) 409–417.
[25] A. Goldmann, F. Dinkelacker, Approximation of laminar flame characteristics on premixed ammonia/hydrogen/nitrogen/air mixtures at elevated temperatures and pressures, Fuel 224 (2018) 366–378.
[26] O. Mathieu, E.L. Petersen, Experimental and modeling study on the high-temperature oxidation of ammonia and related NOx chemistry, Combust. Flame 162 (2015) 554–570.
[27] E. Salzano, A. Basco, F. Cammarota, V. Di Sarli, A. Di Benedetto, Explosions of syngas/CO_2 mixtures in oxygen-enriched air, Ind. Eng. Chem. Res. 51 (2012) 7671–7678.
[28] H.A. Yepes, A.A. Amell, Laminar burning velocity with oxygen-enriched air of syngas produced from biomass gasification, Int. J. Hydrogen Energy 38 (2013) 7519–7527.
[29] X. Cai, J.H. Wang, W.J. Zhang, Y.L. Xie, M. Zhang, Z.H. Huang, Effects of oxygen enrichment on laminar burning velocities and Markstein lengths of $CH_4/O_2/N_2$ flames at elevated pressures, Fuel 184 (2016) 466–473.
[30] J.H. Lee, J.H. Kim, J.H. Park, O.C. Kwon, Studies on properties of laminar premixed hydrogen-added ammonia/air flames for hydrogen production, Int. J. Hydrogen Energy 35 (2010) 1054–1064.
[31] J.H. Lee, S.I. Lee, O.C. Kwon, Effects of ammonia substitution on hydrogen/air flame propagation and emissions, Int. J. Hydrogen Energy 35 (2010) 11332–11341.
[32] P. Kumar, T.R. Meyer, Experimental and modeling study of chemical-kinetics mechanisms for H_2-NH_3-air mixtures in laminar premixed jet flames, Fuel 108 (2013) 166–176.
[33] J. Li, H. Huang, N. Kobayashi, Z. He, Y. Nagai, Study on using hydrogen and ammonia as fuels: combustion characteristics and NOx formation, Int. J. Energy Res. 38 (2014) 1214–1223.
[34] A. Ichikawa, A. Hayakawa, Y. Kitagawa, K.D. Kunkuma Amila Somarathne, T. Kudo, H. Kobayashi, Laminar burning velocity and Markstein length of ammonia/hydrogen/air premixed flames at elevated pressures, Int. J. Hydrogen Energy 40 (2015) 9570–9578.
[35] H. Takeishi, J. Hayashi, S. Kono, W. Arita, K. Iino, F. Akamatsu, Characteristics of ammonia/N_2/O_2 laminar flame in oxygen-enriched air condition, Trans. JSME 81 (2015) 14–00423 (in Japanese).
[36] Q.M. Liu, X. Chen, J.X. Huang, Y. Shen, Y.M. Zhang, Z.W. Liu, The characteristics of flame propagation in ammonia/oxygen mixtures, J. Hazard. Mater. 363 (2019) 187–196.
[37] G.Q. Wang, Y.Y. Li, W.H. Yuan, Z.B. Zhou, Y. Wang, Z.Z. Wang, Investigation on laminar burning velocities of benzene, toluene and ethylbenzene up to 20 atm, Combust. Flame 184 (2017) 312–323.
[38] K. Kohse-Höinghaus, D.F. Davidson, A.Y. Chang, R.K. Hanson, Quantitative NH2 concentration determination in shock tube laser-absorption experiments, J. Quant. Spectrosc. Radiat. Transf. 42 (1989) 1–17.
[39] D. Bradley, P.H. Gaskell, X.J. Gu, Burning velocities, markstein lengths, and flame quenching for spherical methane-air flames: a computational study, Combust. Flame 104 (1996) 176–198.
[40] M.P. Burke, Z. Chen, Y.G. Ju, F.L. Dryer, Effect of cylindrical confinement on the determination of laminar flame speeds using outwardly propagating flames, Combust. Flame 156 (2009) 771–779.
[41] A.P. Kelley, G. Jomaas, C.K. Law, Critical radius for sustained propagation of spark-ignited spherical flames, Combust. Flame 156 (2009) 1006–1013.
[42] H. Hashemi, J.M. Christensen, S. Gersen, P. Glarborg, Hydrogen oxidation at high pressure and intermediate temperatures: experiments and kinetic modeling, Proc. Combust. Inst. 35 (2015) 553–560.
[43] M.P. Burke, S.J. Klippenstein, Ephemeral collision complexes mediate chemically termolecular transformations that affect system chemistry, Nat. Chem. 9 (2017) 1078–1082.
[44] D.L. Baulch, C.T. Bowman, C.J. Cobos, R.A. Cox, T. Just, J.A. Kerr, M.J. Pilling, D. Stocker, J. Troe, W. Tsang, R.W. Walker, J. Warnatz, Evaluated kinetic data for combustion modeling: supplement ii, J. Phys. Chem. Ref. Data 34 (2005) 757–1397.
[45] V. Samu, T. Varga, I. Rahinov, S. Cheskis, T. Turányi, Determination of rate parameters based on NH_2 concentration profiles measured in ammonia-doped methane-air flames, Fuel 212 (2018) 679–683.
[46] A. Fontijn, S.M. Shamsuddin, D. Crammond, P. Marshall, W.R. Anderson, Kinetics of the HH reaction with H_2 and reassessment of HNO formation from NH+CO_2, H_2O, Combust. Flame 145 (2006) 543–551.
[47] J.C. Mackie, G.B. Bacskay, Quantum chemical study of the mechanism of reaction between nh (X 3Σ-) and H_2, H_2O, and CO_2 under combustion conditions, J. Phys. Chem. A 109 (2005) 11967–11974.
[48] D.P. Linder, X.F. Duan, M. Page, Ab initio variational transition state theory calculations for the H+NH_2<=>H_2+NH hydrogen abstraction reaction on the triplet potential energy surface, J. Phys. Chem. 99 (1995) 11458–11463.
[49] I. Rahinov, A. Goldman, S. Cheskis, Absorption spectroscopy diagnostics of amidogen in ammonia-doped methane/air flames, Combust. Flame 145 (2006) 105–116.
[50] D.P. Linder, X.F. Duan, M. Page, Thermal rate constants for R+N_2H_2=>RH+N_2H (R=H, OH, NH_2) determined from multireference configuration interaction and variational transition state theory calculations, J. Chem. Phys. 104 (1996) 6298–6307.

[51] J.J. Zheng, R.J. Rocha, M. Pelegrini, L.F.A. Ferrão, E.F.V. Carvalho, O. Roberto-Neto, F.B.C. Machado, D.G. Truhlar, A product branching ratio controlled by vibrational adiabaticity and variational effects: kinetics of the H+trans-N_2H_2 reactions, J. Chem. Phys. 136 (2012) 184310.
[52] J.A. Miller, C.T. Bowman, Mechanism and modeling of nitrogen chemistry in combustion, Prog. Energy Combust. Sci. 15 (1989) 287–338.
[53] A.M. Dean, J.W. Bozzelli, Combustion chemistry of nitrogen, in: W.C. Gardiner (Ed.), Gas-Phase Combustion Chemistry, Springer, New York, 2000, pp. 125–341.
[54] S.J. Klippenstein, L.B. Harding, B. Ruscic, R. Sivaramakrishnan, N.K. Srinivasan, M.-.C. Su, J.V. Michael, Thermal decomposition of NH_2OH and subsequent reactions: ab initio transition state theory and reflected shock tube experiments, J. Phys. Chem. A 113 (2009) 10241–10259.
[55] Chemkin-Pro 15092, Reaction Design, San Diego, 2009.
[56] E.J. Hu, Z.H. Huang, J.J. He, H.Y. Miao, Experimental and numerical study on laminar burning velocities and flame instabilities of hydrogen-air mixtures at elevated pressures and temperatures, Int. J. Hydrogen Energy 34 (2009) 8741–8755.
[57] E. Varea, V. Modica, A. Vandel, B. Renou, Measurement of laminar burning velocity and markstein length relative to fresh gases using a new postprocessing procedure: application to laminar spherical flames for methane, ethanol and isooctane/air mixtures, Combust. Flame 159 (2012) 577–590.
[58] C. Duynslaegher, H. Jeanmart, J. Vandooren, Flame structure studies of premixed ammonia/hydrogen/oxygen/argon flames: experimental and numerical investigation, Proc. Combust. Inst. 32 (2009) 1277–1284.
[59] G. Dayma, P. Dagaut, Effects of air contamination on the combustion of hydrogen-effect of NO and NO_2 addition on hydrogen ignition and oxidation kinetics, Combust. Sci. Technol. 178 (2006) 1999–2024.
[60] C.K. Law, Combustion physics, Cambridge University Press, 2006.
[61] F.N. Egolfopoulos, C.K. Law, Chain mechanisms in the overall reaction orders in laminar flame propagation, Combust. Flame 80 (1990) 7–16.
[62] M. Goswami, S.C.R. Derks, K. Coumans, W.J. Slikker, M.H. de Andrade Oliveira, R.J.M. Bastiaans, C.C.M. Luijten, L.P.H. de Goey, A.A. Konnov, The effect of elevated pressures on the laminar burning velocity of methane+air mixtures, Combust. Flame 160 (2013) 1627–1635.
[63] G.Q. Wang, Y.Y. Li, W.H. Yuan, Y.Z. Wang, Z.B. Zhou, Y.Z. Liu, J.H. Cai, Investigation on laminar flame propagation of n-butanol/air and n-butanol/O_2/He mixtures at pressures up to 20 atm, Combust. Flame 191 (2018) 368–380.